Bioconjugate Chemistry

Article

pubs.acs.org/bc

Self-Assembling Doxorubicin–Tocopherol Succinate Prodrug as a New Drug Delivery System: Synthesis, Characterization, and *in Vitro* and *in Vivo* Anticancer Activity

Nicolas Duhem,[‡,⊥] Fabienne Danhier,[‡,⊥] Vincent Pourcelle,[†] Jean-Marc Schumers,[§] Olivier Bertrand,[§] Cécile S. LeDuff,[†] Stephanie Hoeppener,[#] Ulrich S. Schubert,[#] Jean-François Gohy,[§] Jacqueline Marchand-Brynaert,[†] and Véronique Préat*[,‡]

[‡]Université catholique de Louvain, Louvain Drug Research Institute, Pharmaceutics and Drug Delivery, 73 B1.73.12 Avenue Mounier, 1200 Brussels, Belgium

[†]Université catholique de Louvain, Institute of Condensed Matter and Nanosciences, Molecules, Solids and Reactivity, Place L. Pasteur, 1, L4.01.02, 1348 Louvain-la-Neuve, Belgium

[§]Université catholique de Louvain, Institute of Condensed Matter and Nanosciences, Bio and Soft Matter, Place L. Pasteur, 1, L4.01.01, 1348 Louvain-la-Neuve, Belgium

[#]Laboratory of Organic and Macromolecular Chemistry, Friedrich Schiller University Jena, Humboldtstrasse 10, 07743 Jena, Germany

Supporting Information

ABSTRACT: Self-assembled prodrugs forming nanoaggregates are a promising approach to enhance the antitumor efficacy and to reduce the toxicity of anticancer drugs. To achieve this goal, doxorubicin was chemically conjugated to D-α-tocopherol succinate through an amide bond to form *N*-doxorubicin–α-D-tocopherol succinate (N-DOX–TOS). The prodrug self-assembled in water into 250 nm nanostructures when stabilized with D-α-tocopherol poly(ethylene glycol) 2000 succinate. Cryo-TEM analysis revealed the formation of nanoparticles with a highly ordered lamellar inner structure. NMR spectra of the N-DOX–TOS nanoparticles indicated that N-DOX–TOS is located in the core of the nanoparticles while PEG chains and part of the tocopherol are in the corona. High drug loading (34% w/w) and low *in vitro* drug release were achieved. *In vitro* biological assessment showed significant anticancer activity and temperature-dependent cellular uptake of N-DOX–TOS nanoparticles. *In vivo*, these nanoparticles showed a greater antitumor efficacy than free DOX. N-DOX–TOS nanoparticles might have the potential to improve DOX-based chemotherapy.

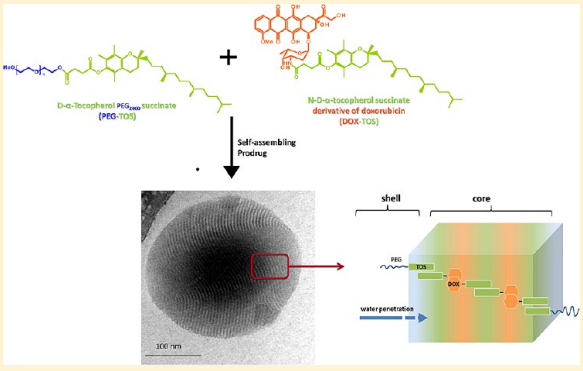

INTRODUCTION

Doxorubicin (DOX) is a highly effective and widely used chemotherapeutic agent against various types of cancers including breast cancers, urothelial cancers, hematopoietic malignancies, and other solid tumors.[1] DOX causes DNA damage and induction of apoptosis through the inhibition of topoisomerase II and stabilization of a ternary drug–topoisomerase II (TOPO II)–DNA complex.[2] Its effectiveness is limited by its short half-life in the bloodstream and its cytotoxicity in normal tissues. The cumulative dose of DOX is limited to 500–600 mg/m^2 to avoid cardiotoxicity, while it should be increased for tumor treatment.[1,3,4] Therefore, there is a need to find an efficient way to deliver DOX to increase its activity and to limit its toxicity.

Utilization of nanomedicines in oncology has attracted the attention of many research endeavors in recent years. Nanomedicines provide better biopharmaceutical properties to anticancer drugs. They can decrease their toxicity and side effects, improve their bioavailability and stability, and prolong their circulation time.[1,5−7] Moreover, nanomedicines can passively accumulate in tumors through the enhanced permeation and retention (EPR) effect.[8]

One major limitation of most of the nanocarriers is the low drug loading efficiency, that is, low weight ratio of drug/nanocarrier. Hence, amphiphilic prodrugs that self-assemble and form nanostructures have been designed.[9] Prodrugs when administered must be chemically or enzymatically degraded *in vivo* to the parent active drug, preferably in a controlled or predictable manner.[5] Lipid–drug conjugates and polymer–drug conjugates have extensively been investigated as prodrugs for cancer treatment and have shown promising results in preclinical and some clinical studies.[9−11] Self-assembled

Received: July 12, 2013
Revised: November 20, 2013
Published: December 11, 2013

 © 2013 American Chemical Society

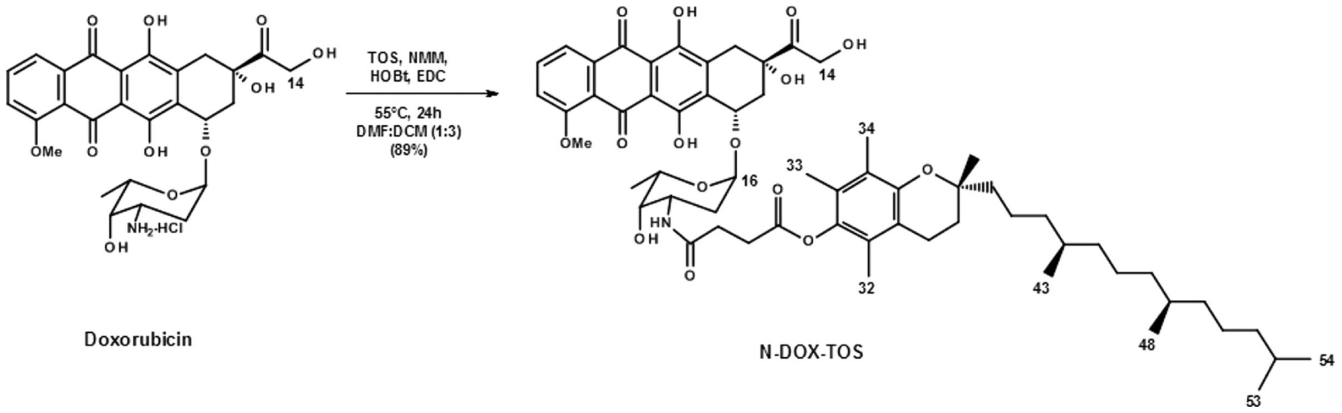

Figure 1. Synthesis of N-DOX−TOS.

prodrug-based delivery can be an answer to common prodrug limitations. Harnessing the advantages of prodrug and nanomedicine strategies in cancer therapy can lead to strongly efficient therapeutic options to achieve (i) maximum drug loading efficiency, (ii) controlled and prolonged release kinetics, and (iii) passive targeting to the tumor. In particular, the lipid squalene has been chemically conjugated with various therapeutic molecules to construct nanoassemblies of 100−300 nm that are promising for cancer treatment.[12−14]

In this paper, we applied the self-assembled prodrug-based delivery concept to DOX. We have developed a vitamin E derivative of doxorubicin, *N*-doxorubicin−α-D-tocopherol succinate (N-DOX−TOS). Vitamin E derivatives are particularly promising for the formation of anticancer drug conjugates. Besides the nontoxic and biocompatible characteristics of the vitamin E family, the synergic ability of D-α-tocopherol succinate (TOS) to act with a chemotherapeutic drug, improving tumor response to chemotherapy, has been demonstrated.[15] TOS has been found to inhibit the proliferation of various cancer cells *in vitro* and *in vivo*. Cells that can respond to antitumor effects mediated by TOS include *inter alia* human neuroblastoma cells, prostate carcinoma cells, promyelotic cells, gastric cancer cells, and breast cancer cells.[15−18] Previous experiment in our laboratory have shown that when TOS was grafted on glucosamine, the derivative spontaneously self-assembled in water in the presence of D-α-tocopheryl poly(ethylene glycol) 1000 succinate (TPGS) acting as a stabilizer, by using a simple nanoprecipitation method (unpublished data).

The aim of this study was to develop N-DOX−TOS nanoparticles in order to increase the anticancer effect, to decrease the side effects of the parent drug, or both. An amido prodrug (N-DOX−TOS) was synthesized, and the effectiveness of the TOS conjugation on the drug was determined by ^{1}H NMR, ^{13}C NMR, mass spectrometry, and HPLC. The physicochemical characteristics of N-DOX−TOS formulated as nanoparticles such as size and morphology of the supramolecular structures were explored. The *in vitro* cytotoxicity, the cellular uptake, and the mechanisms of uptake of the N-DOX−TOS nanoparticles were determined by using the MCF-7 breast cancer cell line. Finally, preliminary *in vivo* studies were performed in CT-26 tumor-bearing mice.

EXPERIMENTAL SECTION

Materials. All solvents, including anhydrous solvents, and reagents were purchased from Acros Organics, Alfa Aesar, Fluka, Sigma-Aldrich, or VWR, and used without any further purification. Deuterated solvents were purchased from Eurisotop (France). Doxorubicin hydrochloride (DOX, USP31 standard) was purchased from Chemieliva Pharmaceutical (China). α-Tocopherol succinate (TOS) was purchased from Sigma. All reactions under dry conditions were performed under argon atmosphere in flame-dried glassware. Poly(ethylenoxide) monomethyl ether (PEO45-OH) (M_n = 2000 g/mol) was dried by azeotropic cycles with toluene prior to use. Dichloromethane (DCM) was distilled over CaH_2, and TOS was dried 24 h in a vacuum oven at 35 °C prior to use.

Instrumentation. ^{1}H (500 MHz) and ^{13}C (125 MHz) NMR spectra were recorded on a Bruker Avance 500 spectrometer. Spectra were obtained in $CDCl_3$, $(CD_3)_2SO$, or D_2O at room temperature. Chemical shifts, δ, are reported in ppm and are calibrated on the solvent residual signal at 7.26 and 77.16 for $CDCl_3$ and at 2.50 and 39.52 for $(CD_3)_2SO$. For NMR spectra acquired in D_2O, trimethylsilyl-3-propionic acid-d_4-sodium salt was used as reference (0 ppm). NMR coupling constants (J) are reported in hertz. High resolution mass spectrometry (HRMS) analyses were performed using a QExactive equipment (Thermo Scientific). TLC analysis was performed on Merck silica gel 60 F_{254} with detection under UV light, and flash chromatography was performed on silica gel (40−60 mesh) purchased from Rocc (Belgium). The HPLC system consisted of a Waters (Waters, USA) Alliance 2699 separation module combined with a Waters 2998 photodiode array detector, a Waters 600 pump, a Waters 717 autosampler, and Waters 486 absorbance detector. Analytical separations were performed with a Waters XBridge C18 column (4.6 mm × 50 mm, 2.5 μm) equipped with a conventional precolumn. HPLC analyses were performed at a temperature of 25 °C with a volume of full-loop injections of 5 μL. The flow rate was 1 mL·min^{-1}. Detection was performed at 254/280 nm, and online UV/vis absorbance scans were performed. For N-DOX−TOS, a MeOH/H_2O gradient was applied (from 1:1 to 1:0).

Synthesis of *N*-D-α-Tocopherol Succinate Derivative of Doxorubicin. The *N*-D-α-tocopherol succinate derivative of doxorubicin (N-DOX−TOS) was synthesized by covalent coupling of DOX with TOS onto the amino group of the glucosamine (Figure 1). DOX·HCl (251 mg, 0.43 mmol, 1.20 equiv) was dissolved in warm DMF (5 mL) prior to the addition of *N*-methyl morpholine (51 mg, 0.50 mmol, 1.4 equiv), hydroxybenzotriazole (HOBt; 68 mg, 1.50 mmol, 1.4 equiv), and TOS (191. mg, 0.36 mmol, 1 equiv). Then, (1-ethyl-3(3-(dimethylamino)propyl)carbodiimide hydrochloride

dx.doi.org/10.1021/bc400326y | Bioconjugate Chem. 2014, 25, 72−81

(EDC·HCl) (98 mg, 0.50 mmol, 1.4 equiv) dissolved in DCM (15 mL) was added dropwise to the reaction mixture under stirring, and the solution was heated at 55 °C for 24 h. DCM (20 mL) was then added, and the reaction mixture was washed four times with 60 mL of brine. Then the organic layer was dried on $MgSO_4$, filtered, evaporated, and dried under vacuum for 24 h. The resulting red powder (yield 336 mg, 88%, HPLC purity ≥98%) was collected.

^{1}H NMR (500 MHz, $CDCl_3$): δ 0.83 (m, 6H), 0.86 (d, 6H, J = 7 Hz), 1.05−1.13 (m, 6H), 1.2 (s, 3H), 1.24 (m, 10H), 1.27 (d, 3H, J = 6 Hz), 1.36 (m, 3H), 1.51 (m, 2H), 1.72 (m, 2H), 1.8 (m, 2H), 1.91 (s, 3H), 1.95 (s, 3H), 2.04 (s, 3H), 2.15 (dd, 1H, J = 14 Hz. J = 4 Hz), 2.24 (bs, 1H), 2.32 (d, 1H, J = 15 Hz), 2.53 (m, 4H), 2.88 (m, 1H), 2.96 (d, 1H, J = 18 Hz), 2.96 (bs, 1H), 3.03 (bs, 1H), 3.24 (d, 1H, J = 18 Hz), 3.64 (s, 1H), 4.05 (s, 3H), 4.11 (m, 1H), 4.12 (m, 1H), 4.76 (s, 2H), 5.25 (m, 1H), 5.48 (m, 1H), 5.99 (d, 1H, J = 8.3 Hz), 7.37 (d, 1H, J = 8.2 Hz), 7.76 (dd, 1H, J = 8.1 Hz), 8 (d, 1H, J = 8.1 Hz).^{13}C NMR (125 MHz, $CDCl_3$): δ 11.9, 12.3, 13.1, 17, 19.8, 19.9, 20.7, 21.1, 22.8, 22.9, 24, 24.6, 24.9, 28.1, 29.3, 29.8, 31.2, 32.8, 32.9, 34.1, 35.8, 37.4, 37.6, 39.5, 40.2, 45.6, 56.8, 65.7, 67.3, 69.2, 69.8, 75.2, 76.7, 100.9, 111.5, 111.7, 117.5, 118.5, 119.9, 120.9, 123.1, 125, 126.7, 133.7, 135.6, 135.9, 140.5, 149.5, 155.7, 156.3, 161.1, 170.8, 171.9, 186.7, 187.1, 214. HRMS-ESI (m/z): $[M + Na]^+$ calculated for $C_{60}H_{81}NO_{15}Na$ 1078.54984, found 1078.54992.

Synthesis of D-α-Tocopherol Polyethylene 2000 Succinate. Under argon, a solution of dicyclocarbodiimide (DCC) (189 mg, 0.92 mmol, 1.2 equiv) in dry DCM (5 mL) was added dropwise, at 0 °C to a stirred mixture of PEO_{45}-OH (1425 mg, 0.76 mmol, 1.0 equiv), 4-dimethylaminopyridine (DMAP; 11 mg, 0.08 mmol, 0.1 equiv), and TOS (485 mg, 0.92 mmol, 1.2 equiv) in dry DCM (14 mL). The mixture was then slowly warmed to 20 °C. A white precipitate corresponding to the N,N'-dicyclohexyl urea appeared after 20 min of reaction time. The reaction medium was stirred at 20 °C for 18 h. The mixture was filtered in order to remove the precipitate, and the mixture was washed twice with 0.05 M HCl and twice with saturated $NaHCO_3$ solutions.[19] The organic phase was dried over Na_2SO_4 and filtered, and the solvent was removed in vacuo. The residue was dissolved in a minimum of THF and precipitated twice in a diethyl ether/hexane (1:1, v/v) mixture as a white powder, which was further dried in vacuo at 35 °C for 24 h (yield: 1775 mg, 92%).

^{1}H NMR (500 MHz, $CDCl_3$): δ (t, 2H, ^3J = 4.5 Hz, CH_2), 3.64 (brs, 178H, CH_2), 3.37 (s, 3H, CH_3), 2.92 (t, 2H, ^3J = 6.5 Hz, CH_2), 2.79 (t, 2H, ^3J = 6.5 Hz, CH_2), 2.57 (t, 2H, ^3J = 6.5 Hz, CH_2), 2.07 (s, 3H, CH_3), 2.00 (s, 3H, CH_3), 1.96 (s, 3H, CH_3), 1.90−1.65 (m, 2H, CH_2), 1.60−1.00 (m, 24H, CH, CH_2, CH_3), 0.86 (d, 6H, ^3J = 6.5 Hz, CH_3), 0.84 (d, 6H, ^3J = 6.5 Hz, CH_3).

Preparation of DOX−TOS Nanoparticles. The preparation of N-DOX−TOS nanoparticles was performed by using the nanoprecipitation technique.[20] Briefly, a solution of N-DOX−TOS and $TPGS_{2000}$ (2:1 w/w) in acetone was added dropwise under stirring (500 rpm) into 2.5 mL of 5% aqueous glucose solution. Precipitation of the nanoassemblies occurred spontaneously. Acetone was completely evaporated using a Rotavapor to obtain a free suspension of N-DOX−TOS nanoparticles in water (4 mg/mL).[13]

Physicochemical Characteristics of the Nanoparticles. The average N-DOX−TOS nanoparticle size and ζ potential were determined, respectively, by photon correlation spectroscopy and laser Doppler velocimetry, combined with phase analysis light scattering (PALS) using a Zetasizer Nano ZS (Malvern Instruments, U.K.). The instrument was calibrated with reference polystyrene nanoparticles (Malvern Instruments, U.K.). The particle size was also assessed after storage at 4 °C for 6 months. All assays were performed in triplicate.

The loading efficiency (LE) was determined as the amount of DOX equivalents in the N-DOX−TOS nanoparticles.

$$\mathrm{LE} = \frac{\text{Amount of DOX equivalents in nanoparticles}}{\text{Amount of prodrug} + \text{Amount of TPGS}_{2000}}$$

Cryogenic transmission electron microscopy (Cryo-TEM) investigations were conducted on a Philips CM-120. Samples were vitrified in a home-built blotting device in liquid ethane. Samples were transferred in a liquid nitrogen environment into a Gatan 626 holder at temperatures lower than −180 °C and were imaged at low electron doses. The diameter of the observed nanoparticles and the period of the lamellar internal structures were calculated from cryo-TEM pictures by averaging measurements performed on more than 100 objects recorded from different areas on the cryo-TEM grid.

NMR of Nanoparticles in Water. N-DOX−TOS nanoparticles were prepared as described above but using deuterated solvents (i.e., $(CD_3)_2CO$ and D_2O). The final concentration of the system was 4 mg of N-DOX−TOS and 2 mg of $TPGS_{2000}$ in 1 mL of D_2O. The ^{1}H NMR (500 MHz) spectra were acquired at 20 °C with the following experimental settings: delay between scans (D1) of 10 s; 5000 scans (16 h); acquisition time 1.5 s; number of points 24576; spectral window 16 ppm. The HDO signal was suppressed using presaturation prior to measuring the ^{1}H spectrum.

Nanoparticle Stability. To determine the stability of the nanoparticles, 1 mL of N-DOX−TOS nanoparticles made of 1 mg of the prodrug N-DOX−TOS and 0.5 mg of $TPGS_{2000}$ was placed in a 1 mL dialysis bag (molecular mass cutoff 1 kDa, Spectra/Por, Spectrum Laboratory Inc., Canada). The dialysis bag was incubated with gentle stirring in 30 mL of PBS (pH 7.4), which was changed at predetermined time points. The collected dialysate was analyzed by fluorescence (PerkinElmer LS-30, PerkinElmer Ltd., Beaconsfield, U.K., λ_{ex} = 475 nm, λ_{em} = 590 nm). A DOX calibration curve was established (0.04−1 μg/mL). All assays were performed in triplicate.

Cell Experiments. *Cell Lines.* MCF-7 breast adenocarcinoma cells (American Type Culture Collection, ATCC HTB-22) were employed as *in vitro* models for the assessment of DOX and N-DOX−TOS nanoparticles. The cells were cultured in DMEM medium supplemented with 10% FBS, 1% penicillin−streptomycin solution, 1% pyruvate, and 1% glucose (Invitrogen Life technologies, Merelbeke, Belgium).

In Vitro Anticancer Activity of DOX−TOS Nanoparticles. Cytotoxicity of N-DOX−TOS nanoparticles was evaluated in MCF-7 cells and was compared with that of free DOX. Cells were seeded at a density of (8−12) × 10^4 cells/well, depending on the drug incubation time, in 96-well transparent plates and incubated for 24 h. The medium was then replaced by the free DOX or N-DOX−TOS nanoparticles at various drug concentrations. The incubation was carried out for 24, 48, and 72 h. The cell viability was determined by the 1-(4,5-dimethylthiazol-2-yl)-3,5-diphenylformazan (MTT, Sigma) assay. At 24, 48, and 72 h, the medium was removed. MTT (0.5 mg/mL) in medium was added, and the cells were incubated for 3 h. The media was removed from all wells, and

100 μL of DMSO (Merck, Germany) was added to dissolve the formazan byproduct. Absorbance of the 96-well plates was assessed with a Multiscan EX (Thermo Fisher Scientific Corporation, USA) at 620 nm. From the absorbance, the viability of the cells expressed in percentages was calculated using the negative control as reference (100% of viability). Triton (1%) was used as positive control. All assays were performed in triplicate ($N = 3$, $n = 4$). IC_{50} values were calculated using a nonlinear regression (log(inhibitor) versus response, variable slope) in Graphpad prism 5 for Windows.

Cells were also incubated with N-DOX−TOS solutions (DOX concentration = 0.2 mg/mL) at 4 °C for 2 h or at 37 °C. After 2 h, solutions were removed, cells were washed 3 times with PBS, and new culture medium was added. After 24 h of incubation at 37 °C, cells were then incubated for additional 3 h with DMEM containing MTT (5 mg/mL). The MTT test was assessed as aforementioned.

Cellular Uptake by Fluorescence Microscopy. MCF-7 cells were cultured in 12-well plates containing a small glass plate precoated with 100 μL of polylysine at a density of 2×10^5 cells/mL. One day after plating, MCF-7 cells were incubated with N-DOX−TOS nanoparticles or free DOX at 10 μM DOX-equivalent concentration at 37 °C for 24 h. After incubation, medium was removed. Cells were fixed with 4% paraformaldehyde in PBS then washed 3 times with PBS. Cells were incubated 5 min with DAPI (0.1 μg/mL diluted 10^4 times in PBS) and washed three times with PBS. Cells were incubated 1 h with concanavalin A−Alexa Fluor 488 conjugate (ConA; 1/200 in PBS, v/v) and then washed three times with PBS. Finally cells were mounted on Vectashield (Vector Lab Inc., USA) and examined with a fluorescence microscope (Axio Imager 2, Zeiss) using the 350 nm (DAPI, blue), 488 nm (ConA, green), and 595 nm (DOX, red) filters and photographed with an AxioCam MRc5 camera (Zeiss, Germany).

In Vivo Experiments on Antitumor Efficacy of N-DOX−TOS. All experiments were performed in compliance with guidelines set by national regulations and were approved by the ethical committee for animal care of the health science sector of the Université catholique de Louvain.

CT26 cells (5×10^4 cells per mouse) were injected subcutaneously in the right flank of BALB/c mice (Janvier, Genest-St-Isle, France) to allow easy and reproducible tumor volume measurements. Mice were randomly assigned to a treatment group when tumor reached a volume of 27 ± 5 mm^3. Treatment was injected trough the tail vein.[21] Three groups were defined (six mice per group): group 1 PBS injection; group 2 injection of N-DOX−TOS nanoparticles (DOX dose, 10 mg/kg); group 3 injection of free DOX (DOX dose, 10 mg/kg). The effect of N-DOX−TOS nanoparticles on tumor growth was assessed by daily measurements of tumor volume with an electronic caliper. The end point of the experiment was determined as the moment when tumor reached 600 mm^3. At this point, mice were sacrificed.

Statistics. Statistical analyses were completed using Graphpad prism 5 for Windows. IC_{50} values were compared with a two-way ANOVA with a Bonferroni post-test. *In vivo* experiments were expressed as mean ± SEM and analyzed using two-way ANOVA, Bonferroni post-test, and Kaplan−Meier survival rate.

RESULTS

Synthesis and Characterization of the N-DOX−TOS. As shown on Figure 1, the prodrug of DOX based on tocopherol conjugation, namely, *N*-doxorubicin−D-α-tocopherol succinate (N-DOX−TOS), was synthesized using a classical carbodiimide coupling method to bind the carboxylic acid of TOS to the amino group of DOX. An excess of DOX was used to drive the coupling reaction to completion and to allow simple purification by successive washings with brine. This strategy demonstrated to be successful since the N-DOX−TOS prodrug was obtained in high purity (≥98% from HPLC). The exclusive linkage of TOS onto the amine group of DOX was unambiguously established by proton and carbon NMR (1D and 2D experiments, that is, HMBC and HMQC).

We similarly synthesized $TPGS_{2000}$ by linking tocopherol succinate to PEG of a molar mass of 2000 g·mol^{-1} via an ester bond as described elsewhere.[22]

Table 1. Size Analysis of DOX−TOS Nanoparticles ($N = 3$)

	Z, average diameter (nm)	PDI
freshly synthesized nanoparticles	234 ± 12	0.101 ± 0.035
nanoparticle stability after 6 months (4 °C)	245 ± 8	0.074 ± 0.027

Formulation of DOX−TOS Nanoparticles. The TOS derivative of DOX was designed to form anticancer nanoparticles with (i) high drug loading (>30%), (ii) self-assembling properties and easy manufacture, and (iii) size adapted to intravenous injection and to the EPR effect to passively target DOX in the tumor.[8,23]

N-DOX−TOS alone was able to self-assemble in water, but the nanoparticles tended to form large aggregates. Hence, a PEGylated vitamin E derivative was added as a stabilizer to their formulation. PEGylation is known to stabilize nanoparticles by steric hindrance. $TPGS_{2000}$ was chosen because it has been previously demonstrated that $TPGS_{2000}$-based micelles were more stable than the $TPGS_{1000}$ ones bearing shorter PEG chains.[22] Longer PEG chains are helpful to avoid elimination via the reticuloendothelial system by reducing the protein interactions on the surface, thus preventing opsonin binding,[24] extending blood circulation times and reducing liver accumulation. Finally, PEG bearing targeting units, such as folate, antibodies, or peptides, can be introduced in order to have targeted drug delivery systems.[22]

The nanoparticles were obtained by using a simple nanoprecipitation method, which consists in adding an acetone solution of N-DOX−TOS and $TPGS_{2000}$ dropwise in water under stirring and then evaporating acetone under vacuum. $TPGS_{2000}$ was mandatory to stabilize the molecular structuration of the nanoparticles. TPGS might act as a stabilizer due to its amphiphilic character: a hydrophilic PEG chain and a hydrophobic tocopherol head anchored in the lipidic part of the nanoparticle.[25]

In contrast to DOX solution, the dispersion appeared as an opaque, milky red solution (see Supporting Information, S1). The best ratio of N-DOX−TOS/$TPGS_{2000}$ was 2:1 with a maximum concentration of 4 mg/mL of the prodrug to ensure the stability of the solution. At this concentration, corresponding to a DOX concentration of approximately 2 mg/mL, the N-DOX−TOS nanoparticles are in the concentration range of Doxil, a commercially available liposomal formulation of DOX.[26]

The amount of DOX loaded in the N-DOX−TOS nanoparticles was 34 wt %. This is one of the highest loading efficiencies reported for DOX delivery systems. For instance, recently a DOX−TPGS prodrug was synthesized with a drug

dx.doi.org/10.1021/bc400326y | *Bioconjugate Chem.* 2014, 25, 72−81

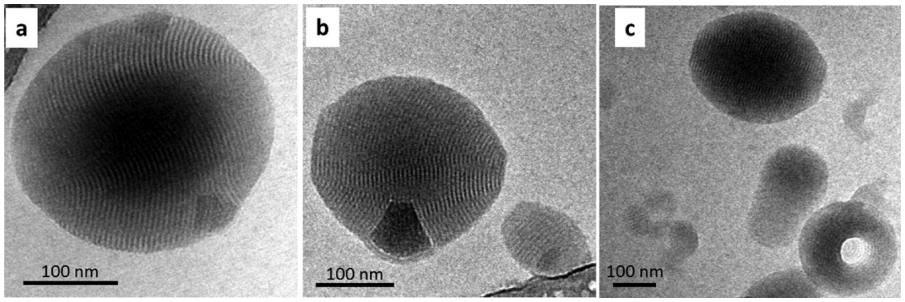

Figure 2. Cryo-TEM of N-DOX−TOS nanoparticles showing a spherical nanoparticle (a), a rugby ball shaped nanoparticle (b), and a donut shaped nanoparticle (c).

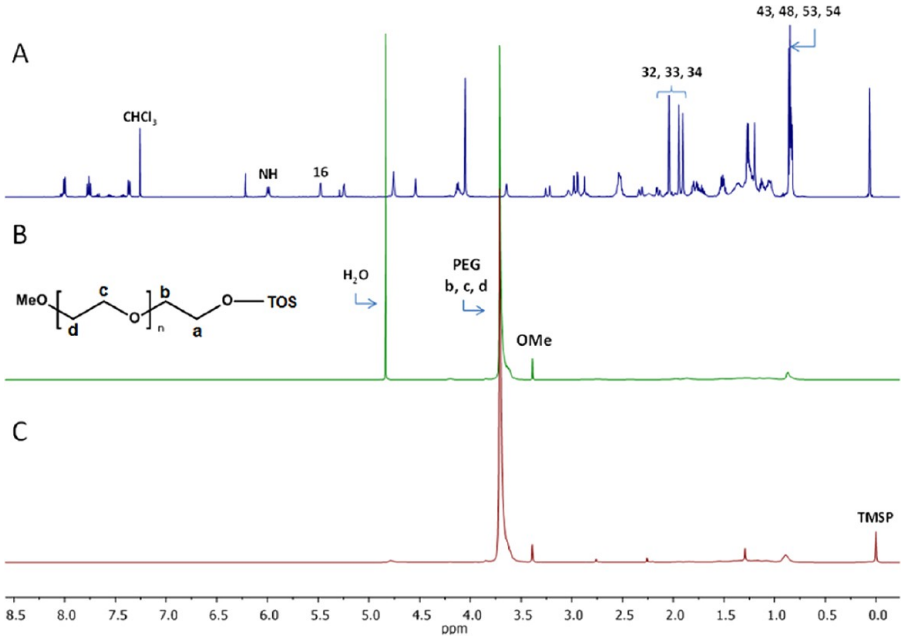

Figure 3. Stacked ^{1}H NMR full spectra of (A) N-DOX−TOS in $CDCl_3$, (B) TPGS in D_2O, and (C) nanoparticles containing N-DOX−TOS and TPGS in D_2O with presaturation of H_2O protons.

loading of 26 wt %.[19] Another example with a star-shaped copolymer of lysine-linked di-$TPGS_{2000}$ (PLV2K) self-assembled in nanostructures of 16 nm was characterized by a 9.5 wt % drug loading.[27] Our N-DOX−TOS nanoparticle drug loading is also 1−7 times higher than that of PLGA nanoparticles loaded or conjugated with DOX.[28−30] Compared with nanomagnetite/squalenoyl doxorubicin (USPIO/SQdox), a theragnostic system composed of DOX prodrug, the N-DOX−TOS nanoparticle payload was 47% higher.[31] A PEGylated prodrug of DOX (PEG−DOX) forming nanoparticles of 125 nm was recently synthesized and showed a superior drug loading (46%) in comparison to N-DOX−TOS nanoparticles.[32]

Physicochemical Characteristics of the DOX−TOS Nanoparticles. The hydrodynamic diameter of the nanoparticles estimated by DLS was 234 nm for a 4 mg/mL prodrug concentration solution. The polydispersity in size was narrow (see Table 1). The ζ potential of the nanoparticles was −4.1 ± 0.7 mV. Since DOX−TOS nanoparticles have phenol and carboxylic acid functions, one can assume that at neutral pH, part of the carboxylic acid groups is ionized and that (part of) the resulting carboxylate anions have a tendency to localize at the surface of the nanoparticles. This should lead to a slightly negative ζ potential as observed experimentally. These results suggest that N-DOX−TOS nanoparticles meet size and surface characteristics necessary to develop an injectable anticancer nanomedicine. To reach the tumor site effectively, nanoparticle size should be much less than 400 nm (more likely 150−200 nm) to diffuse through the tumor interstitium, and the particle charge should be neutral or anionic to efficiently evade renal elimination.[23]

The N-DOX−TOS nanoparticles were analyzed using cryo-TEM. Rather monodisperse nanoparticles with a diameter of 250 ± 30 nm were observed throughout the whole sample (Figure 2a). The characteristic size of these nanoparticles is in perfect in agreement with the hydrodynamic diameter measured by DLS. Other morphologies including rugby ball and donut-like nanoparticles were occasionally observed (Figure 2b,c), again with average sizes around 250 nm. All these morphologies display an internal lamellar substructure with a characteristic period of 5.5 ± 0.5 nm visualized as alternating dark and clear bands in the cryo-TEM pictures. This points toward a hierarchical self-assembly process in the investigated N-DOX−TOS nanoparticles. Particles with a nanostructured internal organization have been previously described for the so-called cubosomes. Cubosomes are dispersed particles of bicontinuous cubic liquid crystalline phase that are physically stable in an excess of water.[33] From

dx.doi.org/10.1021/bc400326y | *Bioconjugate Chem.* 2014, 25, 72−81

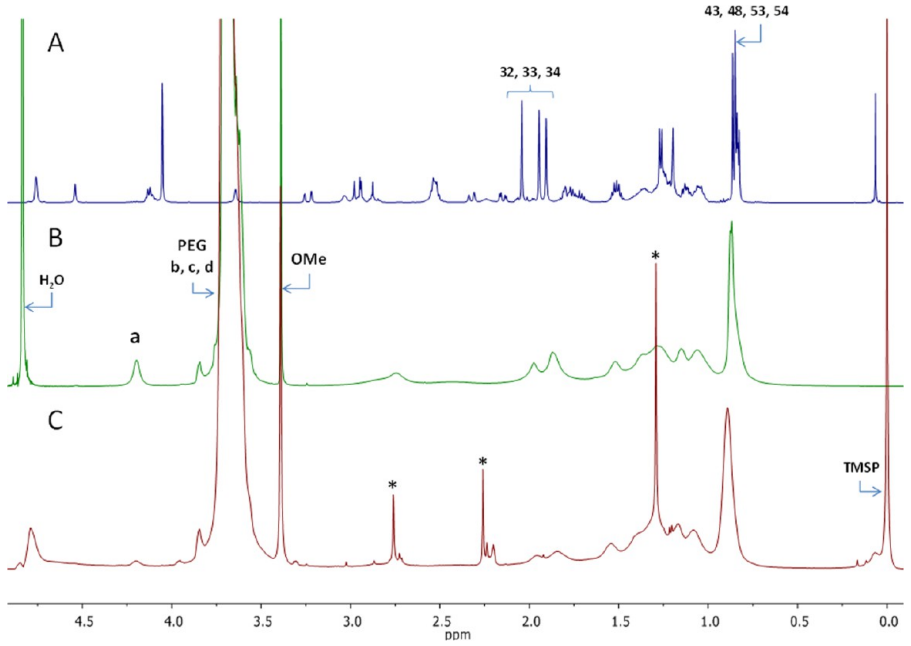

Figure 4. Stacked ^{1}H NMR spectra zoomed on the 0−4.75 ppm section: (A) N-DOX−TOS in $CDCl_3$, (B) TPGS in D_2O, and (C) nanoparticles containing N-DOX−TOS and TPGS in D_2O with presaturation of H_2O protons (∗ indicates unidentified impurities removed by dialysis).

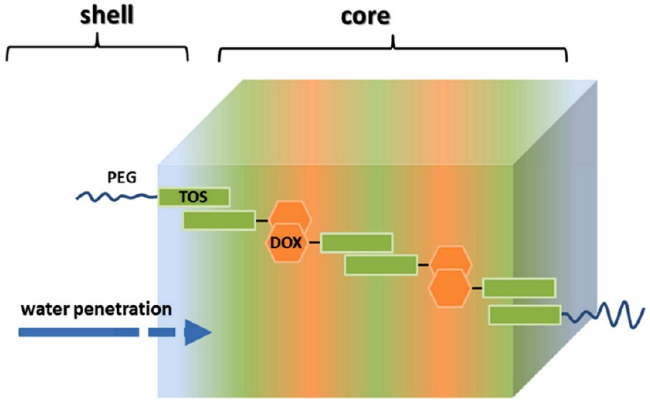

Figure 5. Schematic representation of N-DOX−TOS nanoparticle structure based on the ^{1}H NMR spectrum interpretation.

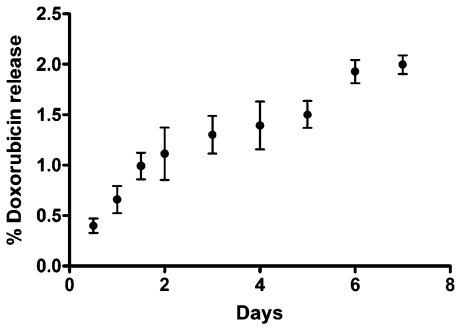

Figure 6. Release of doxorubicin from N-DOX−TOS (n = 3).

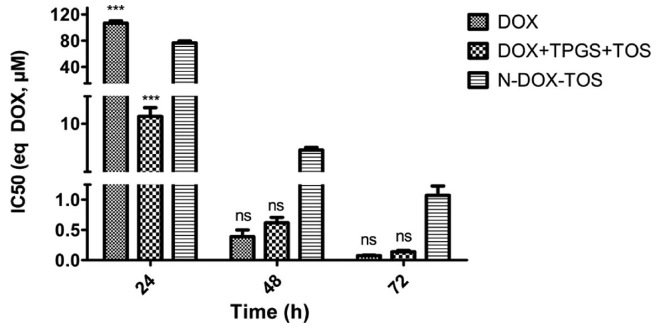

Figure 7. IC_{50} values of DOX, DOX + TPGS + TOS, and N-DOX−TOS nanoparticles in DOX equivalent. Statistical differences are shown using N-DOX−TOS as a benchmark (*** = $p < 0.001$; ns means $p > 0.05$, vs N-DOX−TOS; N = 3, n = 4).

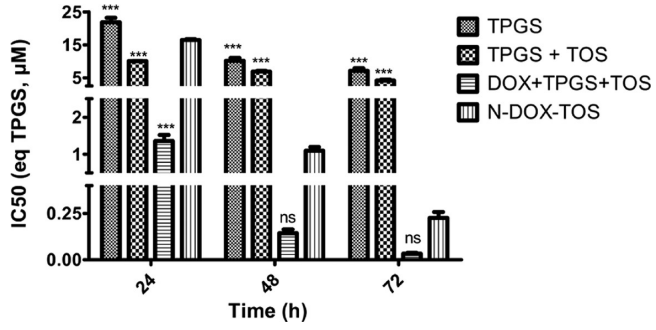

Figure 8. IC_{50} values of TPGS, TPGS + TOS, DOX + TPGS + TOS and N-DOX−TOS nanoparticles in TPGS equivalent. Statistical differences are shown using N-DOX−TOS as a benchmark (*** = $p <$ 0.001, ns means $p > 0.05$, vs N-DOX−TOS; N = 3, n = 4).

the examination of a large number of the nanostructured objects formed by N-DOX−TOS, it however appears that the internal structure of our nanoparticles is not compatible with the cubic structure of cubosomes but is rather characteristic of a lamellar organization (Figure 2). Basically, surfactant molecules are known to self-organize into three types of organization: spheres, cylinders, and lamellae. The alternating dark and clear lamellae observed in Figure 2 should contain on one hand the DOX aromatic part and on the other hand the aliphatic part of TOS. The added stabilizing TGPS molecule should be rejected toward the surface of the nanoparticle to act as stabilizer. NMR studies reported below confirm this hypothesis. To the best of

dx.doi.org/10.1021/bc400326y | Bioconjugate Chem. 2014, 25, 72−81

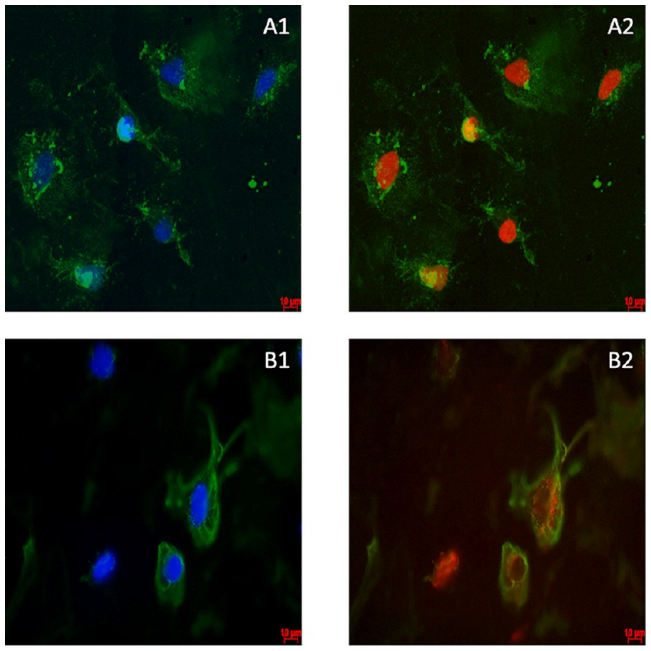

Figure 9. Detection of fluorescent DOX (red) in MCF-7 cells after 24 h incubation with (A) the free DOX and (B) N-DOX–TOS nanoparticles at 10 μM equivalent of DOX. DAPI (blue) and ConA (green) staining were used to label nuclei and membranes, respectively.

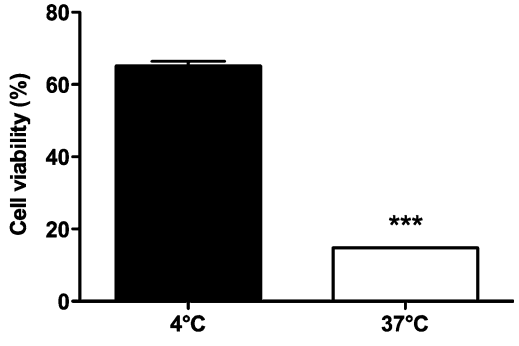

Figure 10. Temperature dependence of N-DOX–TOS in MCF-7 cells after 24 h incubation. Cells were incubated with N-DOX–TOS nanoparticles (DOX concentration = 0.2 mg/mL) at 4 °C for 2 h or at 37 °C. The cell viability was evaluated using a MTT test.

our knowledge, no nanoparticles with an internal lamellar structure were reported so far from tocopherol derivatives. It should be noted that different types of internal nanostructures have been observed for nanoparticles formed by squalenoyl–drug conjugates depending on their chemical structure. For example, gemcitabine–squalene was shown to self-assemble in inverse hexagonal phases resulting from the packing of cylinders of water-swollen gemcitabine molecules surrounded by the hydrophobic squalene moieties. Differently, 2′-3′-dideoxycytidine–squalene was shown to self-assemble in cubosomes.[13,34,35]

To get deeper insight in the structure of the N-DOX–TOS nanoparticles, ^{1}H NMR experiments were performed in D_2O (see Supporting Information, S2). The measured spectrum shows predominance of PEG and tocopherol protons (Figure 3C). The protons of DOX are not visible on the NMR spectrum (Figure 3), indicating that there are no free DOX molecules in the solution but rather that these are located inside the core of the nanoparticles in a collapsed solid state. This suggests an organization of the particles with N-DOX–TOS in the core of the structures where water cannot enter. The external shell of nanoparticles, that is, the part exposed to water, is mostly constituted of PEG and part of the tocopherol linked to it. This is reinforced by the fact that we observe a broadening of tocopherol peaks (comparison between Figure 4, panels A and C). Moreover the integration of the peaks of the aliphatic methyl protons of TOS corresponds only to a small portion of the expected amount. For instance, considering the whole content in TOS, coming from TPGS and N-DOX–TOS contributions, the theoretical ratio of PEG integrals (at 3.71 ppm) to tocopherol methyl protons integrals (at 0.89 ppm) should be of 2.6. Taking into account the integrals of these peaks, we found an experimental ratio of 18.5. This result is close to the ratio calculated for the TOS in a TPGS molecule alone, which is 15.2 (for details, see Supporting Information, S3).

Based on the cryo-TEM and NMR spectra collected on the nanoparticles, we suggest the nanoparticle structure illustrated in Figure 5, where the N-DOX–TOS is located in the core of the nanoparticles with a segregation between DOX and TOS domains giving rise to the alternating lamellae as observed by cryo-TEM, and the TPGS segments pointed out toward the solution to act as stabilizers. Finally, it should be highlighted that the internal lamellar organization in N-DOX–TOS is

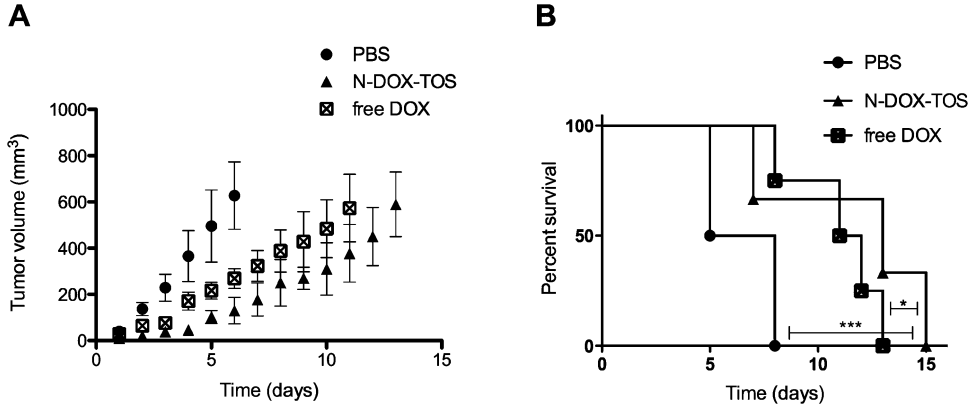

Figure 11. *In vivo* antitumor efficacy. (A) Tumor growth curves in CT-26-tumor bearing mice treated with free DOX, N-DOX–TOS nanoparticles (DOX dose = 10 mg/kg), or untreated mice (PBS). The treatment was injected in the tail vein of mice when tumors reached 27 ± 5 mm^3 (n = 6/group). Results are presented as the mean ± SEM. (B) Survival rates of tumor-bearing mice.

dx.doi.org/10.1021/bc400326y | *Bioconjugate Chem.* 2014, 25, 72–81

different from previously reported cubic and hexagonal packing of cylinders for other systems.

The release of DOX from the N-DOX−TOS nanoparticles was tested in PBS (pH 7.4) during 1 week at 25 °C using a dialysis method. Results showed that it was not possible to quantify any free DOX within 12 h. After 7 days, the amount of DOX released from N-DOX−TOS nanoparticles was less than 2% (Figure 6). The stability of the N-DOX−TOS nanoparticles was investigated at 4 °C during 6 months. No size changes could be observed in comparison with the initial nanoparticles, supporting high long-term stability (Table 1). This is due to the presence of the PEG aqueous layer, which provides steric hindrance. Thus, these experiments demonstrate that N-DOX−TOS nanoparticles are stable.

Cytotoxicity, Cellular Uptake, and Mechanisms of Transport of N-DOX−TOS Nanoparticles. The cytotoxicity of N-DOX−TOS nanoparticles was assessed *in vitro* on the MCF-7 cell line in comparison with free DOX and the physical mixture of DOX, $TPGS_{2000}$, and TOS (DOX + TPGS + TOS), after 24, 48, and 72 h of culture. MCF-7 breast cancer cell line was chosen as model since the effect of DOX has been extensively studied on this cell line.[19,36,37]

The cytotoxicity of N-DOX−TOS nanoparticles, DOX + TPGS + TOS, and DOX was time-dependent ($p < 0.01$). The IC_{50} of DOX, DOX + TPGS + TOS, and N-DOX−TOS are shown in Figure 7 (data in Supporting Information, S4). IC_{50} values of DOX were similar to those previously reported.[19] The differences between DOX solution, DOX + TPGS + TOS, and N-DOX−TOS nanoparticles in inhibiting growth of MCF-7 cells was highly significant ($p < 0.001$) after 24 h. No significant difference was observed within three groups after 48 ($p > 0.05$) and 72 h ($p > 0.05$).

The prodrug nanoparticles exhibited higher cytotoxicity after 24 h in comparison to DOX. This advantage was not shown for longer times of cell incubation. After 48 and 72 h, N-DOX−TOS nanoparticles were less toxic than the free drug and the components of the nanoparticles (DOX + TPGS + TOS). The higher toxicity of N-DOX−TOS nanoparticle in comparison to DOX after 24 h might be due to the activity of the released vitamin E derivatives. It has been found that TOS and TPGS are able to induce apoptosis and to increase antitumor effect.[18,38−40] These data were confirmed on MCF-7 cells as shown in Figure 8 (data in Supporting Information, S5). Synergistic effect between DOX and vitamin E derivatives was clearly observed after 24 h when cells were incubated with DOX + TPGS + TOS. However, this effect was no longer significant after 48 and 72 h. N-DOX−TOS nanoparticles were less effective than DOX + TPGS + TOS after 24 h, which might indicate an incomplete or delayed conversion to the parent drug. The lower cytotoxicity of N-DOX−TOS nanoparticles after 48 h and 72 h may be explained for the same reasons. This is a common limitation of hydrophobic prodrugs since their applicability depends on their susceptibility to hydrolytic or enzymatic activation. This is consistent with the high stability of amide derivatives as shown in studies on PEG−DOX derivatives.[41]

The cellular uptake of DOX and N-DOX−TOS nanoparticles was qualitatively investigated by microscopy after 24 h of incubation with MCF-7 cells (Figure 9). The free DOX was totally distributed in the nucleus of the cells since the colors of the DAPI-labeled nucleus (Figure 9A1) and the DOX (Figure 9A2) can be perfectly overlaid. N-DOX−TOS nanoparticles were characterized by a cytosolic and nuclear distribution with red detection inside and around the nucleus (Figure 9B1,B2). The change in intracellular distribution could play a significant role for the activity of the drug as was already reported for TPGS−DOX conjugates and PEG−DOX.[19] The delivery of the prodrug nanoparticles into the cells may occur in a different way from that of the free drug. This may considerably influence the mode of action and the toxicity of the N-DOX−TOS nanoparticles.[19]

Finally, mechanisms of uptake of N-DOX−TOS nanoparticles were briefly evaluated. Hence we assessed the temperature dependence of uptake comparing incubation of N-DOX−TOS at 4 and 37 °C because it is well established that at 4 °C pinocytic/endocytic uptake is inactivated.[42] As shown in Figure 10, the cell viability was drastically enhanced when N-DOX−TOS was incubated on cells at 4 °C, indicating a lower uptake and suggesting that an active transport is involved in this uptake.

***In Vivo* Antitumor Efficacy.** The *in vivo* antitumor efficacy of N-DOX−TOS nanoparticles compared with free DOX was evaluated in CT26-tumor-bearing mice (Figure 11). All treatments induced a higher delay in tumor growth than the control group (Figure 11A). Moreover, N-DOX−TOS nanoparticles induced a higher regrowth delay when compared with free DOX (Figure 11A). Kaplan−Meier survival rate was performed (Figure 11B). N-DOX−TOS nanoparticles and free DOX exhibited higher survival rates than the untreated group (PBS) with median survival rates of 13 and 11.5 days, respectively, compared with 6.5 days ($p < 0.001$). Additionally, N-DOX−TOS nanoparticles and free DOX presented significantly different median survival times ($p < 0.05$). These results suggest than N-DOX−TOS nanoparticles could be an interesting formulation of DOX.

■ CONCLUSION

Our objective was to develop self-assembling prodrug of DOX and vitamin E with a high drug loading to take advantage of the EPR effect of nanoparticulate systems and the biological activity of vitamin E derivatives. The new DOX prodrug self-assemble into nanoparticles showing an internal lamellar microphase separated structure in the presence of TPGS as stabilizer. N-DOX−TOS is located in the core of the nanoparticles, while PEG chains are in the corona. A high drug loading (34%) and low *in vitro* drug release, compatible with DOX clinical use, were achieved. Significant cytotoxic activity and cellular uptake of N-DOX−TOS nanoparticles were observed. Temperature dependence of uptake suggests that the main mechanism of N-DOX−TOS nanoparticles uptake occurs by active diffusion. *In vivo*, these nanoparticles showed a greater antitumor efficacy than free DOX. Our design of nanomedicines consisting of N-DOX−TOS and TPGS could provide a sustained and passively targeted DOX delivery, which might reduce DOX toxicity *in vivo*. Studies are ongoing to further confirm this hypothesis.

■ ASSOCIATED CONTENT

Ⓢ Supporting Information

Nanoparticles of N-DOX-TOS/TPGS in water after evaporation of acetone, interpretation of NMR spectra of N-DOX−TOS nanoparticles, integral theoretical calculation for the determination of TOS in the nanoparticles and in TGPS, IC_{50} values of DOX, N-DOX−TOS nanoparticles, and DOX + TPGS + TOS in equivalent micromolar DOX, and IC_{50} values of TPGS, TPGS + TOS, N-DOX−TOS nanoparticles and DOX + TPGS + TOS in equivalent micromolar TPGS. This

dx.doi.org/10.1021/bc400326y | *Bioconjugate Chem.* 2014, 25, 72−81

material is available free of charge via the Internet at http://pubs.acs.org.

AUTHOR INFORMATION

Corresponding Author

*Tel: +32 2 764 73 09. Fax: +32 2 764 73 98, E-mail: veronique.Preat@uclouvain.be.

Author Contributions

⊥N. Duhem and F. Danhier contributed equally. N. Duhem, F. Danhier, V. Pourcelle, J. Marchand-Brynaert, and V. Préat designed the research; N. Duhem, V. Pourcelle, J.-M. Schumers, S. Hoeppener, and O. Bertrand performed research; N. Duhem, F. Danhier, V. Pourcelle, J.-F. Gohy, J. Marchand-Brynaert, and V. Préat analyzed data; and N. Duhem, F. Danhier, V. Pourcelle, and V. Préat wrote the paper.

Notes

The authors declare no competing financial interest.

ACKNOWLEDGMENTS

The authors express their thanks to Télévie, FSR (Université Catholique de Louvain), and Région Wallonne for financial support and fellowships to Nicolas Duhem and the Fond National pour la Recherche Scientifique (FNRS) to Fabienne Danhier. We thank Laurent Collard for the HPLC analyses.

ABBREVIATIONS

ConA, concanavalin A; Cryo-TEM, cryo-transmission electron microscopy; DAPI, 4′-6-diamidino-2-phenylindole; DCC, *N*,*N*′-dicyclocarbodiimide; DCM, dichloromethane; DLS, dynamic light scattering; DMAP, 4-dimethylaminopyridine; DMEM, Dulbecco's modified Eagle medium; DMF, dimethylformamide; DMSO, dimethyl sulfoxide; DOX, doxorubicin; EDC·HCl, 1-ethyl-3-(3-(dimethylamino)propyl)carbodiimide HCl; FBS, fetal bovine serum; HOBt, hydroxybenzotriazole; HPLC, high-performance liquid chromatography; MTT, 1-(4,5-dimethylthiazol-2-yl)-3,5-diphenylformazan; NMM, *N*-methylmorpholine; PBS, phosphate buffered saline; PEO_{45}-OH, poly(ethylene oxide) mono methyl ether; PFA, paraformaldehyde; TEA, triethylamine; TOS, α-D-tocopherol succinate

REFERENCES

(1) Huan, M. L., Zhou, S. Y., Teng, Z. H., Zhang, B. L., Liu, X. Y., Wang, J. P., and Mei, Q. B. (2009) Conjugation with alpha-linolenic acid improves cancer cell uptake and cytotoxicity of doxorubicin. *Bioorg. Med. Chem. Lett. 19*, 2579−2584.

(2) Aroui, S., Brahim, S., Waard, M. D., and Kenani, A. (2010) Cytotoxicity, intracellular distribution and uptake of doxorubicin and doxorubicin coupled to cell-penetrating peptides in different cell lines: A comparative study. *Biochem. Biophys. Res. Commun. 391*, 419−425.

(3) Chhikara, B. S., St. Jean, N., Mandal, D., Kumar, A., and Parang, K. (2011) Fatty acyl amide derivatives of doxorubicin: synthesis and in vitro anticancer activities. *Eur. J. Med. Chem. 46*, 2037−2042.

(4) Talelli, M., Morita, K., Rijcken, C. J., Aben, R. W., Lammers, T., Scheeren, H. W., van Nostrum, C. F., Storm, G., and Hennink, W. E. (2011) Synthesis and characterization of biodegradable and thermosensitive polymeric micelles with covalently bound doxorubicin-glucuronide prodrug via click chemistry. *Bioconjugate Chem. 22*, 2519−2530.

(5) Fang, J. Y., and Al-Suwayeh, S. A. (2012) Nanoparticles as delivery carriers for anticancer prodrugs. *Expert Opin. Drug Delivery 9*, 657−669.

(6) She, W., Luo, K., Zhang, C., Wang, G., Geng, Y., Li, L., He, B., and Gu, Z. (2013) The potential of self-assembled, pH-responsive nanoparticles of mPEGylated peptide dendron-doxorubicin conjugates for cancer therapy. *Biomaterials 34*, 1613−1623.

(7) Wong, A. D., DeWit, M. A., and Gillies, E. R. (2012) Amplified release through the stimulus triggered degradation of self-immolative oligomers, dendrimers, and linear polymers. *Adv. Drug Delivery Rev. 64*, 1031−1045.

(8) Danhier, F., Feron, O., and Préat, V. (2010) To exploit the tumor microenvironment: Passive and active tumor targeting of nanocarriers for anti-cancer drug delivery. *J. Controlled Release 148*, 135−146.

(9) Vemula, P. K., Campbell, N. R., Zhao, F., Xu, B., John, G., and Karp, J. M. (2011) *Comprehensive Biomaterials*, pp 339−355, Elsevier, Oxford.

(10) Gong, X., Moghaddam, M. J., Sagnella, S. M., Conn, C. E., Danon, S. J., Waddington, L. J., and Drummond, C. J. (2011) Lyotropic liquid crystalline self-assembly material behavior and nanoparticulate dispersions of a phytanyl pro-drug analogue of capecitabine-a chemotherapy agent. *ACS Appl. Mater. Interfaces 3*, 1552−1561.

(11) Tang, H., Murphy, C. J., Zhang, B., Shen, Y., Sui, M., Van Kirk, E. A., Feng, X., and Murdoch, W. J. (2010) Amphiphilic curcumin conjugate-forming nanoparticles as anticancer prodrug and drug carriers: In vitro and in vivo effects. *Nanomedicine (London, U.K.) 5*, 855−865.

(12) Bildstein, L., Pili, B., Marsaud, V., Wack, S., Meneau, F., Lepetre-Mouelhi, S., Desmaele, D., Bourgaux, C., Couvreur, P., and Dubernet, C. (2011) Interaction of an amphiphilic squalenoyl prodrug of gemcitabine with cellular membranes. *Eur. J. Pharm. Biopharm. 79*, 612−620.

(13) Couvreur, P., Reddy, L. H., Mangenot, S., Poupaert, J. H., Desmaele, D., Lepetre-Mouelhi, S., Pili, B., Bourgaux, C., Amenitsch, H., and Ollivon, M. (2008) Discovery of new hexagonal supramolecular nanostructures formed by squalenoylation of an anticancer nucleoside analogue. *Small 4*, 247−253.

(14) Reddy, L. H., Ferreira, H., Dubernet, C., Mouelhi, S. L., Desmaele, D., Rousseau, B., and Couvreur, P. (2008) Squalenoyl nanomedicine of gemcitabine is more potent after oral administration in leukemia-bearing rats: study of mechanisms. *Anticancer Drugs 19*, 999−1006.

(15) Prasad, K. N., Kumar, B., Yan, X. D., Hanson, A. J., and Cole, W. C. (2003) Alpha-tocopheryl succinate, the most effective form of vitamin E for adjuvant cancer treatment: a review. *J. Am. Coll. Nutr. 22*, 108−117.

(16) Kline, K., Yu, W., and Sanders, B. G. (2004) Vitamin E and breast cancer. *J. Nutr. 134*, 3458S−3462S.

(17) Pussinen, P. J., Lindner, H., Glatter, O., Reicher, H., Kostner, G. M., Wintersperger, A., Malle, E., and Sattler, W. (2000) Lipoprotein-associated alpha-tocopheryl-succinate inhibits cell growth and induces apoptosis in human MCF-7 and HBL-100 breast cancer cells. *Biochim. Biophys. Acta 1485*, 129−144.

(18) Zhang, X., Peng, X., Yu, W., Hou, S., Zhao, Y., Zhang, Z., Huang, X., and Wu, K. (2011) Alpha-tocopheryl succinate enhances doxorubicin-induced apoptosis in human gastric cancer cells via promotion of doxorubicin influx and suppression of doxorubicin efflux. *Cancer Lett. 307*, 174−181.

(19) Cao, N., and Feng, S. S. (2008) Doxorubicin conjugated to D-alpha-tocopheryl polyethylene glycol 1000 succinate (TPGS): Conjugation chemistry, characterization, in vitro and in vivo evaluation. *Biomaterials 29*, 3856−3865.

(20) Reddy, L. H., Dubernet, C., Mouelhi, S. L., Marque, P. E., Desmaele, D., and Couvreur, P. (2007) A new nanomedicine of gemcitabine displays enhanced anticancer activity in sensitive and resistant leukemia types. *J. Controlled Release 124*, 20−27.

(21) Schleich, N., Sibret, P., Danhier, P., Ucakar, B., Laurent, S., Muller, R. N., Jérôme, C., Gallez, B., Préat, V., and Danhier, F. (2013) Dual anticancer drug/superparamagnetic iron oxide-loaded PLGA-based nanoparticles for cancer therapy and magnetic resonance imaging. *Int. J. Pharm. 447*, 94−101.

(22) Mi, Y., Liu, Y., and Feng, S. S. (2011) Formulation of docetaxel by folic acid-conjugated d-alpha-tocopheryl polyethylene glycol

succinate 2000 (Vitamin E TPGS(2k)) micelles for targeted and synergistic chemotherapy. *Biomaterials 32*, 4058−4066.
(23) Steichen, S. D., Caldorera-Moore, M., and Peppas, N. A. (2012) A review of current nanoparticle and targeting moieties for the delivery of cancer therapeutics. *Eur. J. Pharm. Sci. 48*, 416−427.
(24) Brigger, I., Dubernet, C., and Couvreur, P. (2002) Nanoparticles in cancer therapy and diagnosis. *Adv. Drug Delivery Rev. 54*, 631−651.
(25) Zhang, Z., Tan, S., and Feng, S. S. (2012) Vitamin E TPGS as a molecular biomaterial for drug delivery. *Biomaterials 33*, 4889−4906.
(26) Huober, J., Fett, W., Nusch, A., Neise, M., Schmidt, M., Wischnik, A., Gerhardt, S., Goehler, T., Luck, H. J., and Rost, A. (2010) A multicentric observational trial of pegylated liposomal doxorubicin for metastatic breast cancer. *BMC Cancer 10*, No. 2.
(27) Wang, J., Sun, J., Chen, Q., Gao, Y., Li, L., Li, H., Leng, D., Wang, Y., Sun, Y., Jing, Y., Wang, S., and He, Z. (2012) Star-shape copolymer of lysine-linked di-tocopherol polyethylene glycol 2000 succinate for doxorubicin delivery with reversal of multidrug resistance. *Biomaterials 33*, 6877−6888.
(28) Lei, T., Srinivasan, S., Tang, Y., Manchanda, R., Nagesetti, A., Fernandez-Fernandez, A., and McGoron, A. J. (2011) Comparing cellular uptake and cytotoxicity of targeted drug carriers in cancer cell lines with different drug resistance mechanisms. *Nanomedicine 7*, 324−332.
(29) Park, J., Fong, P. M., Lu, J., Russell, K. S., Booth, C. J., Saltzman, W. M., and Fahmy, T. M. (2009) PEGylated PLGA nanoparticles for the improved delivery of doxorubicin. *Nanomedicine 5*, 410−418.
(30) Yoo, H. S., Lee, K. H., Oh, J. E., and Park, T. G. (2000) In vitro and in vivo anti-tumor activities of nanoparticles based on doxorubicin-PLGA conjugates. *J. Controlled Release 68*, 419−431.
(31) Arias, J. L., Reddy, L. H., Othman, M., Gillet, B., Desmaele, D., Zouhiri, F., Dosio, F., Gref, R., and Couvreur, P. (2011) Squalene based nanocomposites: A new platform for the design of multifunctional pharmaceutical theragnostics. *ACS Nano 5*, 1513−1521.
(32) Gou, P. W., Mao, W., Tang, J., Shena, Y., and Sui, M. (2013) Self-assembling doxorubicin prodrug forming nanoparticles for cancer chemotherapy: synthesis and anticancer study in vitro and in vivo. *J. Mater. Chem. B 1*, 284−292.
(33) Spicer, P. T. (2005) Progress in liquid crystalline dispersions: Cubosomes. *Curr. Opin. Colloid Interface Sci. 10*, 274−279.
(34) Caron, J., Maksimenko, A., Wack, S., Lepeltier, E., Bourgaux, C., Morvan, E., Leblanc, K., Couvreur, P., and Desmaele, D. (2013) Improving the antitumor activity of squalenoyl-paclitaxel conjugate nanoassemblies by manipulating the linker between paclitaxel and squalene. *Adv. Healthcare Mater. 2*, 172−185.
(35) Desmaele, D., Gref, R., and Couvreur, P. (2012) Squalenoylation: A generic platform for nanoparticular drug delivery. *J. Controlled Release 161*, 609−618.
(36) Shieh, M. J., Hsu, C. Y., Huang, L. Y., Chen, H. Y., Huang, F. H., and Lai, P. S. (2011) Reversal of doxorubicin-resistance by multifunctional nanoparticles in MCF-7/ADR cells. *J. Controlled Release 152*, 418−425.
(37) Tevyashova, A., Sztaricskai, F., Batta, G., Herczegh, P., and Jeney, A. (2004) Formation of squaric acid amides of anthracycline antibiotics. Synthesis and cytotoxic properties. *Bioorg. Med. Chem. Lett. 14*, 4783−4789.
(38) Guo, Y., Luo, J., Tan, S., Otieno, B. O., and Zhang, Z. (2013) The applications of vitamin E TPGS in drug delivery. *Eur. J. Pharm. Sci. 49*, 175−186.
(39) Turanek, J., Wang, X. F., Knotigova, P., Koudelka, S., Dong, L. F., Vrublova, E., Mahdavian, E., Prochazka, L., Sangsura, S., Vacek, A., Salvatore, B. A., and Neuzil, J. (2009) Liposomal formulation of alpha-tocopheryl maleamide: In vitro and in vivo toxicological profile and anticancer effect against spontaneous breast carcinomas in mice. *Toxicol. Appl. Pharmacol. 237*, 249−257.
(40) Youk, H. J., Lee, E., Choi, M. K., Lee, Y. J., Chung, J. H., Kim, S. H., Lee, C. H., and Lim, S. J. (2005) Enhanced anticancer efficacy of alpha-tocopheryl succinate by conjugation with polyethylene glycol. *J. Controlled Release 107*, 43−52.
(41) Rodrigues, P. C., Beyer, U., Schumacher, P., Roth, T., Fiebig, H. H., Unger, C., Messori, L., Orioli, P., Paper, D. H., Mulhaupt, R., and Kratz, F. (1999) Acid-sensitive polyethylene glycol conjugates of doxorubicin: Preparation, in vitro efficacy and intracellular distribution. *Bioorg. Med. Chem. 7*, 2517−2524.
(42) Tomoda, H., Kishimoto, Y., and Lee, Y. C. (1989) Temperature effect on endocytosis and exocytosis by rabbit alveolar macrophages. *J. Biol. Chem. 264*, 15445−15450.